Nuclear Materials and Energy 33 (2022) 101287

Contents lists available at ScienceDirect

Nuclear Materials and Energy

journal homepage: www.elsevier.com/locate/nme

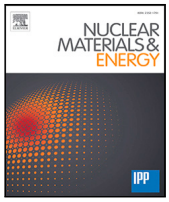

Laser ablation molecular isotopic spectroscopy: A novel tool to characterise the distribution of ^{13}C and ^{12}C on graphite after $^{13}CH_4$ tracer injection in Wendelstein 7-X

E. Wüst [*], T. Dittmar, C. Kawan, J. Romazanov, S. Brezinsek, the W7-X team [1]

Forschungszentrum Jülich, Institut für Energie- und Klimaforschung Plasmaphysik, 52425 Jülich, Germany

ARTICLE INFO

Keywords:
LAMIS
LIBS
W7-X

ABSTRACT

Wendelstein 7-X (W7-X) operation with inertially cooled graphite Test Divertor Unit (TDU) was finalised in a series of identical hydrogen plasmas with injection of 13C isotopically marked methane. The break-up of 13CH4, injected through gas inlets at one toroidal position of W7-X, and the subsequent transport and deposition of 13C in the device was studied ex-situ. The TDU was therefore extracted from the vessel and some of the removed TDU elements were examined regarding their 13C distribution in deposited layers on the surface using Laser Ablation Molecular Isotopic Spectroscopy (LAMIS). This study shows the 13C/12C distinction capabilities of LAMIS used to analyse the carbon deposition pattern on Plasma-Facing Components (PFCs) on two of the removed TDU elements. The resulted pattern was compared with complementary results from Nuclear Reaction Analysis (NRA) and simulations of 13C deposition by ERO2.0, a material transport and plasma-surface interaction code. Ultra- short laser pulses of a Nd:YAG laser were used in collinear double-pulse configuration for LAMIS. The first pulse (l1 = 355 nm, t1 = 35 ps, F = 2.3 J/cm^2) produced a laser- induced plasma on the surface and 50 ns later, the second laser pulse (l2 = 1064 nm, t2 = 35 ps) was directed into this plasma to enhance the signal. Each pulse pair ablates in total 200 nm of the surface material. The analysis is conducted in 1.5 mbar N2 environment for improved signal-to-noise ratio relative to vacuum conditions. A high throughput custom-made spectrometer in Littrow-arrangement (f = 750 mm, A = 6000 at l = 473 nm, lspan = 14 nm) was used to analyse the C2 Swan bands (d3⊓g - a3⊓u, v = 1 to v' = 0) of laser-induced plasma emission.

1. Introduction

Effects of plasma–wall interaction such as erosion of and deposition on Plasma-Facing Components (PFCs) are important for questions of material life time, operational regime and safety of fusion devices. In purely toroidal symmetry, as is present in tokamaks, several studies have been conducted to investigate all of those aspects [1]. The aim for continuous operation of stellarators in complex 3D geometry make new studies in such devices necessary. Mayer et al. [2] observed the erosion and deposition patterns in Wendelstein 7-X (W7-X) with marker layers embedded in PFCs. Codes like ERO2.0 [3] are being developed to simulate plasma–wall interaction in fusion devices. Additional studies of carbon migration leading to deposition in stellarators are needed to test the codes in question and give valuable input for their further development [4].

Experiments in Operation Phase (OP) 1.2b of W7-X had been conducted for this reason, in which ^{13}C isotopically marked methane was injected into a hydrogen plasma [4]. The distribution of deposited ^{13}C on PFCs part of the non-actively cooled fine grain graphite Test Divertor Unit (TDU) are now analysed in post-mortem studies with the components removed from the machine. Methods like Nuclear Reaction Analysis (NRA) or Secondary Ion Mass Spectroscopy (SIMS) are established techniques that have been used for deposition and erosion analyses using marker layers or injecting marker isotopes into the plasma [5,6]. However, Divertor Units are currently completely exchanged for actively water cooled elements to be used in the up-coming OP of W7-X [7,8]. The structure supplying the coolant to the divertor units will make removal for post-mortem analyses more challenging. Accordingly, the development of a method for carbon isotope distinction that can be used in-situ without removal of PFCs is of interest for future studies of carbon migration in a full carbon device in steady-state.

* Corresponding author.
E-mail address: e.wuest@fz-juelich.de (E. Wüst).

[1] The full list of W7-X team members is given in Thomas Sunn Pedersen et al. 2022 Nucl. Fusion 62 042022.

https://doi.org/10.1016/j.nme.2022.101287
Received 10 August 2022; Received in revised form 3 October 2022; Accepted 21 October 2022
Available online 27 October 2022

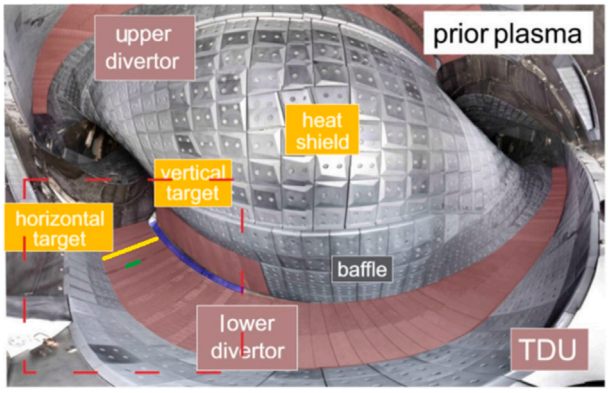

Fig. 1. Picture of the TDU in W7-X before usage. In the marked area, location of injection (green), location of the nearest analysed TDU element (yellow) and the pumping gap (blue) are shown. (For interpretation of the references to colour in this figure legend, the reader is referred to the web version of this article.)

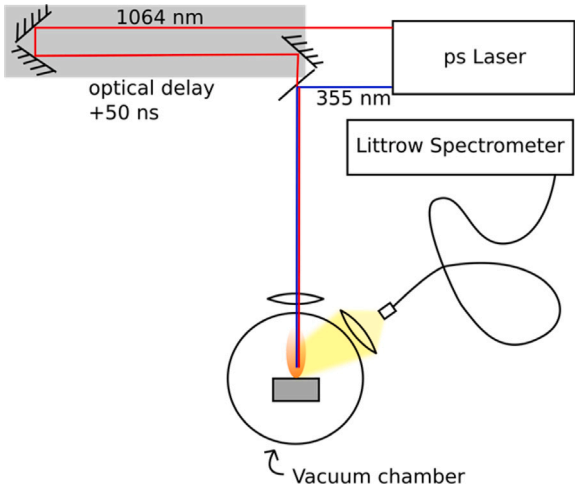

Fig. 2. Schematic of the LAMIS setup with laser system, vacuum chamber and spectrometer.

One potential method for in-situ analysis of material compositions is Laser-Induced Breakdown Spectroscopy (LIBS) [9,10]. LIBS permits to distinguish between different hydrogen isotopes through the observation of isotopic shifts in the spectra emitted by the laser-induced plasma [11]. But the very small isotopic shift in emission from atomic carbon is more challenging to resolve due to the higher nuclear mass, as low light detection limit and the ability to observe multiple spectroscopic lines are required for LIBS. For instance, the isotopic shift of CI line at 505.2 nm is only 0.001 78 nm. A potential solution to this challenge is to observe the emission not from atomic carbon but from diatomic molecules containing carbon such as C_2, CO, CH or CN, that are also present in the plasma [12,13]. This method is called Laser Ablation Molecular Isotopic Spectroscopy (LAMIS) and the following analyses utilise the molecule C_2, which is present in a laser-induced plasma produced on a carbon surface without the need for impurities such as Oxygen, Nitrogen or Hydrogen.

LAMIS is essentially LIBS for molecules released during the ablation process, and therefore a valid option for such an in-situ technique. This text will show the suitability of LAMIS for the measurement of carbon isotope distributions on graphite PFCs with a post-mortem study. We will first describe the gas injection experiment and setup used for ex-situ analysis. Next, the method for analysing the spectra to obtain the ^{13}C content in the ablated volume is explained and discussed. Subsequently, a first study on individual PFCs from the TDU will be used to demonstrate the capabilities of LAMIS and the result will be compared to NRA measurements of ^{13}C depth and spatial resolution and finally compared to simulations with the ERO2.0 code. ERO2.0 is a Monte Carlo impurity transport and PWI code utilising a plasma background from plasma boundary solver EMC3-EIRENE.

2. Experimental

W7-X is a Helias-type stellarator with five-fold toroidal symmetry represented by 5 modules denoted with the index 1 to 5. Each module has a lower and an upper divertor unit each with multiple vertical and horizontal divertor modules containing multiple target elements (see Fig. 1). The presented analyses were done on two target elements from the horizontal, lower divertor of modules 3 and 5. They are labelled as TE01 of HM39TM200h and TE07 of HM58TM200h.

Prior to extraction, $^{13}CH_4$ was injected into a hydrogen plasma through gas valves in the lower TDU of module 3 in the last plasma experiment of OP1.2b. No further plasmas were run before the extraction of TDU elements. The gas nozzles were situated between target elements TE04 and TE05 of divertor module HM39TM200h. About 4×10^{22} molecules were injected during a series of H plasmas in standard divertor configuration accumulating 330 s of plasma duration [4]. Minimum distance between gas nozzles and the closest analysed divertor finger is 165 mm in toroidal direction. Further information about the experiment is given in [4].

Both elements have been extracted at the end of OP 1.2b from the W7-X vessel and cut along poloidal direction into smaller blocks (10 mm toroidal × 25 mm poloidal × 5 mm thick, sometimes smaller in poloidal direction depending on the structure of the surface) which fit into the sample holder of the NRA setup.

The setup used for the ex-situ study presented in this article consists of a laser system including optical elements for delaying laser pulses, the sample chamber with vacuum equipment and the spectrometer including optical elements for light collection (see Fig. 2).

An EKSPLA PL2241CSH-TH Nd:YAG laser generates the 2nd (λ = 532 nm) and 3rd (λ = 355 nm) harmonic of the amplifier output (λ = 1064 nm) and provides laser pulses for the LIBS studies with each of the three wavelengths at different outputs. All three pulses are released at approximately the same time and have a pulse duration of τ = 35 ps. In order to enhance the signal strength, double pulse scheme was used. The laser pulses with wavelengths λ = 355 nm and λ = 1064 nm have been used for the LAMIS measurement. The laser pulse with λ = 355 nm is directly focussed (f = 500 mm) into the sample chamber and thus onto the material's surface. The second laser pulse with λ = 1064 nm is first delayed optically by Δt = 50 ns and then focussed into the plasma generated by the first laser pulse on the material surface. The angle between both beampaths on the surface is $\alpha = 5°$. The crater left behind after ablation by each pulse pair is ~700 μm in diameter and 200 nm in depth.

The experimental chamber is either at vacuum ($p = 10^{-7}$ mbar) or at low pressure (p = 1.5 mbar) filled with nitrogen. The low pressure nitrogen atmosphere enhances emission of the laser-induced plasma for better signal-to-noise-ratio. Outside the chamber at an angle of $\beta = 5°$ to the beampath of the first laser pulse a concave aluminium mirror is used for collection of light, which is then led into a spectrometer by an optical fibre (d =1.5 mm, NA = 0.22). The spectrometer used for spectral analysis is a custom-built spectrometer in littrow arrangement optimised for high ètendue. The ètendue calculates as follows [14]:

$$T = w * h\frac{\pi}{4} * \left(\frac{D}{f}\right)^2 = w * h\frac{\pi}{4} * \left(\frac{1}{N}\right)^2 \quad (1)$$

w is the width of the slit, h the height of the slit and N the focal ratio of the input. A slit width of 50 μm, a slit height of 3 mm and a focal ratio of f/4.3 gives an ètendue of 6.4E3 μm^2 sr. For reference, the spectrometer described in [15] has an ètendue of 30 μm^2 sr. The spectrometer

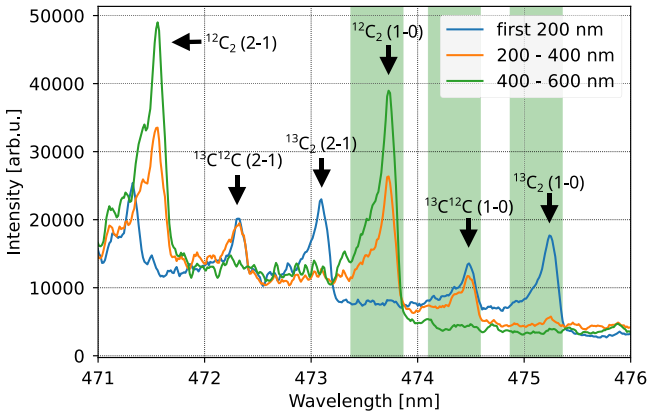

Fig. 3. Blue: spectrum taken from the first 200 nm of a TDU on a position with high ^{13}C content. The content calculated from this spectrum is 84%. orange: spectrum taken from the depth of 200 nm to 400 nm of the same position. The content calculated from this spectrum is 15%. green: spectrum taken from the depth of 400 nm to 600 nm. The content calculated from this spectrum is 0.1%. The content was calculated with Eq. (2). (For interpretation of the references to colour in this figure legend, the reader is referred to the web version of this article.)

observes the wavelength interval 466 nm to 480 nm for an analysis of the 1-0 vibrational bands of the C_2 Swan bands ($d^3\Pi_g \rightarrow a^3\Pi_u$ transition). The spectra were taken 150 ns after first plasma emission and integrated over 5 µs.

The studies provided in this work are conducted under low pressure conditions and the described double pulse configuration does not have benefits for signal-to-noise-ratio under these conditions as the delay between both laser pulses is not at optimum. The benefit lies in the comparison with studies conducted under vacuum conditions for which signal-to-noise-ratio enhancement was seen. These studies are not subject to this article, but will probably be released at a later time.

3. Results

Fig. 3 shows spectroscopic recordings of the C_2 Swan band from the position of highest ^{13}C content taken from the plasmas of the first and second laser pulses respectively. For further analysis, intensities were integrated over a spectroscopic span of 0.5 nm from the band head towards blue (integrated wavelength spans for $^{12}C_2$: 473.37 nm to 473.87 nm, for $^{13}C^{12}C$: 474.10 nm to 474.60 nm and for $^{13}C_2$: 474.83 nm to 475.33 nm). It is assumed that all three isotopologues have the same rovibrational population and emission behaviour. The relative intensities of the three bands carry information about isotopic composition of ablated material with good spatial resolution. If the relative integrated intensities are proportional to the relative abundances of the isotopologues, then the content of ^{13}C as fraction of total carbon in the ablated volume, represented by the sum of $^{13}C_2$, $^{12}C_2$ and $^{13}C^{12}C$, can be calculated by:

$$\frac{n_{^{13}C}}{n_C} = \frac{2 \cdot I_{^{13}C_2} + I_{^{13}C^{12}C}}{2 \cdot (I_{^{13}C_2} + I_{^{13}C^{12}C} + I_{^{12}C_2})} \quad (2)$$

Here I is the integrated intensity of the respective bands.

The spectra were fitted with simulated spectra using the program Pgopher, which provides emission spectra simulations of molecule mixtures [16]. The necessary molecular constants of the three C_2 isotopologues were extracted from the ExoMol database [17]. For this, rotational and vibrational temperatures are assumed to be equal and so were emission characteristics of all three isotopologues. In Fig. 4 two sample spectra and their fitted simulations are shown. Fig. 4 (a) shows measured and simulated spectra of a measurement where no ^{13}C was detected. The simulation finds a single rotation and vibrational (rovibrational) temperature of (5200 ± 21) K. The spectrum and fitted

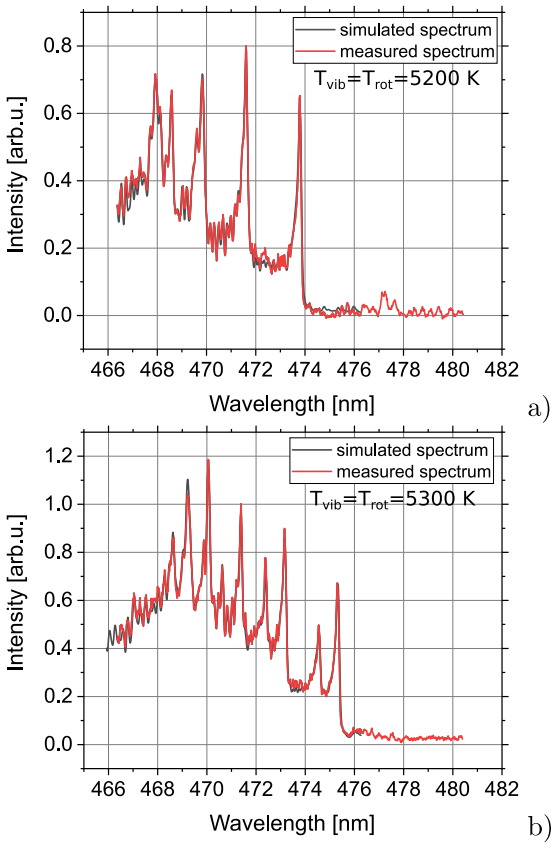

Fig. 4. Spectra from measurements and fitted simulated spectra for (a) a case without ^{13}C and (b) a case with maximum ^{13}C.

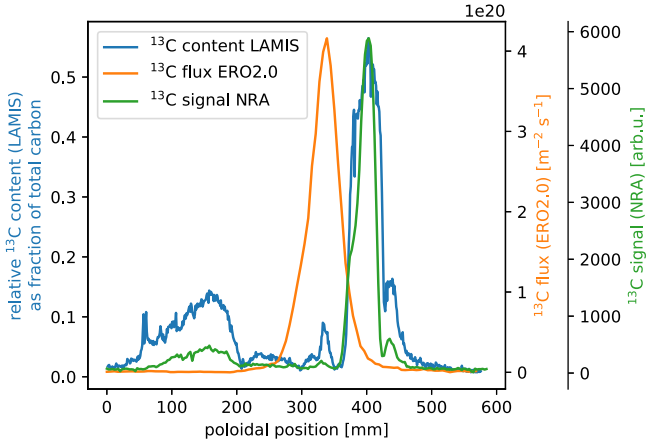

Fig. 5. ^{13}C distribution on TE01 of HM39TM200h as measured by LAMIS, NRA and simulated by ERO2.0.

simulation with highest ^{13}C in this study is presented in Fig. 4 (b). The rovibrational temperature found for this spectrum is (5300 ± 14) K. The given errors are an estimate of the fitting program and probably bigger due to the small fitted spectroscopic interval. Simulations considering CO emission provide similar results. No contribution of CO has been noticed even though Oxygen is a possible impurity in fusion devices. These simulations can provide more information about the LAMIS plasma, but a more detailed analysis is going to be subject of future studies.

The analysed element closer to the injection location was target element TE01 of HM39TM200h. With a distance of minimal 165 mm,

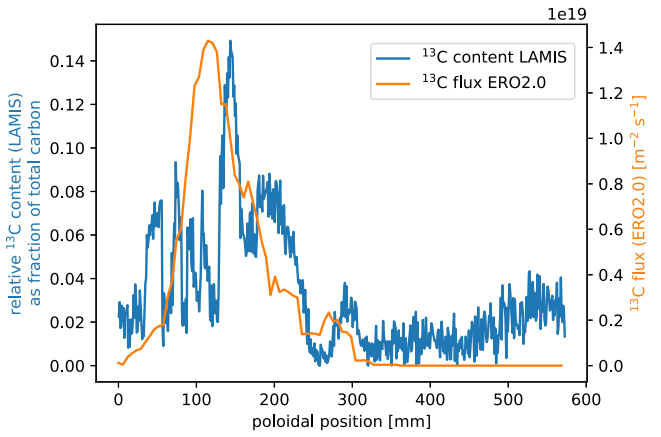

Fig. 6. ^{13}C distribution on TE07 of HM58TM200h as measured by LAMIS and simulated by ERO2.0.

this element was located in the wake of the injection, but not in the zone of strongest direct deposition after dissociation in the plasmas. The ^{13}C distribution as measured by LAMIS and NRA is shown in Fig. 5. The scale on the x-axis shows the poloidal location relative to the pumping gap (cf. Fig. 1). The results of both analyses agree on the position and shape of ^{13}C deposition zones. Maxima in ^{13}C content around 400 mm poloidal coordinate on the target element are due to direct deposition after dissociation of $^{13}CH_4$ in the hot edge plasma of W7-X. A second deposition zone appears between 0 mm to 200 mm poloidal coordinate. No direct deposition from the gas injection is expected here, but ^{13}C can reach this area by dissociation and transport through the plasma including multiple erosion/deposition steps, thus migration. Note that the zone around 150 mm poloidal coordinate reflects the main horizontal strike-line, thus a net erosion zone in normal plasma conditions [4]. Peak ^{13}C deposition in this zone was found at 159 mm poloidal position and is thus slightly further away from the pumping gap than the main erosion zone. The amount of deposited ^{13}C decreases slowly from here towards pumping gap. The causes of ^{13}C deposition in this normally erosion dominated zone have not yet been identified.

The ^{13}C flux onto the element as simulated by ERO2.0 is also shown in Fig. 5. Methane dissociation was taken into account with Janev–Reiter reaction rates [18]. Reflected particles have been subtracted from ^{13}C flux onto the element. For atomic ^{13}C SDTrimSP reflection coefficients were used [19] and for molecules a reflection rate of 1.0 (neutral CH_x) or 0.5 (ionised CH_x) was assumed. The simulation this close to the injection location only takes direct ^{13}C deposition into account. For that reason, ^{13}C content caused by migrating ^{13}C is not predicted. Only the peak in ^{13}C content from direct deposition after injection appears between 270 mm to 410 mm poloidal coordinate. The maxima in simulated ^{13}C and in measured ^{13}C surface content are shifted in poloidal position by about 100 mm. This is probably due to neglection of E × B drift in the simulation or local changes in plasma parameters induced by the injection in its vicinity. Movement of the strike line due to toroidal currents in the plasma is another possible explanation. Further investigations will be done in a modelling focussed paper in the future.

Element TE07 of HM58TM200h was located significantly further away from the injection location, in a different Module, than TE01 of HM39TM200h. ^{13}C content as measured by LAMIS and ^{13}C flux onto the element as simulated by ERO2.0 are shown in Fig. 6. Here, maxima in simulation and measurement are in better agreement than on element TE01 of HM39TM200h, because all ^{13}C being deposited reaches TE07 of HM58TM200h through transport in accordance with background impurities. No direct deposition is expected this far from the injection location.

4. Conclusion

The $^{13}CH_4$ injection into the plasma of W7-X was the last experiment before extraction of the TDU elements. As a result, Deposited ^{13}C is expected to be measured on the TDU surface. The measured distribution matches this expectation even though ^{13}C could only be detected in the topmost two data points of a depth profile.

The ex-situ performed NRA and LAMIS analyses of target element TE01 of TDU module HM39TM200h show generally good agreement on measured ^{13}C distribution. Both analyses were conducted along poloidal lines that were shifted toroidally by about 6 mm, which is expected to be small in relation to the changes in deposition behaviour in this region. The only deviation between the two measurements appears at the position of strong local deposition. The proportion of maximum ^{13}C content in local deposition zone to ^{13}C content in deposition zone caused by migration is higher in NRA results than in LAMIS results. The causes of this difference have not yet been resolved.

Relative to this, the local deposition zone as simulated by ERO 2.0 is shifted for about 100 mm towards the pumping gap. Multiple deposition/erosion steps were not yet taken into account in this simulation. The effort to take into account E × B drift and multiple erosion/deposition steps are ongoing. The observed shift in direct deposition might have been caused by neglection of E × B drift, changes in local plasma parameters induced by the injection or shift of the strike line due to toroidal currents in the plasma. The deposition due to multiple erosion/deposition steps seen on TE07 of divertor module HM58TM200h shows more agreement between simulated and measured ^{13}C deposition. In case the shift of maximum ^{13}C deposition on divertor module HM39TM200h is due to toroidal currents in the plasma, no shift of ^{13}C deposition after multiple erosion/deposition steps is expected on TE07 of HM58TM200h. From the findings so far, we conclude that both, the method proposed for analysing carbon isotope content and the proposed way to analyse Swan bands to access ^{13}C content produce results that are in good agreement with an established way to measure ^{13}C content of PFCs. Although these findings do not demonstrate in-situ utilisation of this method, they do show that this method can determine ^{13}C isotopic content of graphite with high resolution ex-situ. Because LIBS has been utilised for in-situ material analysis [9] and the physics behind LIBS and LAMIS are similar, LAMIS in-situ implementation should be considered for future studies of erosion and deposition in stellarators with actively cooled divertor modules.

CRediT authorship contribution statement

E. Wüst: Investigation, Writing – original draft, Visualization. **T. Dittmar:** Investigation, Resources. **C. Kawan:** Investigation. **J. Romazanov:** Formal analysis. **S. Brezinsek:** Conceptualization, Writing – review & editing, Supervision. **the W7-X team:** Resources.

Declaration of competing interest

The authors declare the following financial interests/personal relationships which may be considered as potential competing interests: Erik Wuest, Timo Dittmar, Christoph Kawan, Juri Ramazonov, Sebastijan Brezinsek reports financial support was provided by European Consortium for the Development of Fusion Energy.

Data availability

Data will be made available on request.

Acknowledgements

This work has been carried out within the framework of the EUROfusion Consortium, funded by the European Union via the Euratom Research and Training Programme (Grant Agreement No 101052200 — EUROfusion). Views and opinions expressed are however those of the author(s) only and do not necessarily reflect those of the European Union or the European Commission. Neither the European Union nor the European Commission can be held responsible for them.

References

[1] R.A. Pitts, J.P. Coad, D.P. Coster, G. Federici, W. Fundamenski, J. Horacek, K. Krieger, A. Kukushkin, J. Likonen, G.F. Matthews, M. Rubel, J.D. Strachan, J.-E. contributors, Material erosion and migration in tokamaks, Plasma Phys. Control. Fusion 47 (12B) (2005) B303–B322.

[2] M. Mayer, M. Balden, S. Brezinsek, V.V. Burwitz, C.P. Dhard, A. Dudek, G. Ehrke, Y. Gao, H. Greuner, R. Guimarães, P. Hiret, S. Klose, R. König, M. Krause, R. Laube, M. Laux, D. Naujoks, R. Neu, J. Oelmann, C. Ruset, T.S. Silva, R. Yi, D. Zhao, W7-X Team, Material erosion and deposition on the divertor of W7-X, Phys. Scr. T171 (2020) 014035.

[3] J. Romazanov, D. Borodin, A. Kirschner, S. Brezinsek, S. Silburn, A. Huber, V. Huber, H. Bufferand, M. Firdaouss, D. Brömmel, B. Steinbusch, P. Gibbon, A. Lasa, I. Borodkina, A. Eksaeva, C. Linsmeier, JET Contributors, First ERO2.0 modeling of Be erosion and non-local transport in JET ITER-like wall, Phys. Scr. T170 (2017) 014018.

[4] S. Brezinsek, C.P. Dhard, M. Jakubowski, R. König, S. Masuzaki, M. Mayer, D. Naujoks, J. Romazanov, K. Schmid, O. Schmitz, D. Zhao, M. Balden, R. Brakel, B. Butterschoen, T. Dittmar, P. Drews, F. Effenberg, S. Elgeti, O. Ford, E. Fortuna-Zalesna, G. Fuchert, Y. Gao, A. Goriaev, A. Hakola, T. Kremeyer, M. Krychowiak, Y. Liang, C. Linsmeier, R. Lunsford, G. Motojima, R. Neu, O. Neubauer, J. Oelmann, P. Petersson, M. Rasinski, M. Rubel, S. Sereda, G. Sergienko, T.S. Pedersen, T. Vuoriheimo, E. Wang, T. Wauters, V. Winters, M. Zhao, R. Yi, Plasma-Surface Interaction in the stellarator W7-X: Conclusions drawn from operation with graphite Plasma-Facing Components, Nucl. Fusion (2021).

[5] M. Mayer, S. Krat, A. Baron-Wiechec, Y. Gasparyan, K. Heinola, S. Koivuranta, J. Likonen, C. Ruset, G. de Saint-Aubin, A. Widdowson, JET Contributors, Erosion and deposition in the JET divertor during the second ITER-like wall campaign, Phys. Scr. T170 (2017) 014058.

[6] J. Likonen, E. Alves, A. Baron-Wiechec, S. Brezinsek, J.P. Coad, A. Hakola, K. Heinola, S. Koivuranta, G.F. Matthews, P. Petersson, M. Rubel, C. Stan-Sion, A. Widdowson, JET-EFDA Contributors, First results and surface analysis strategy for plasma-facing components after JET operation with the ITER-like wall, Phys. Scr. T159 (2014) 014016.

[7] J. Boscary, A. Peacock, R. Stadler, B. Mendelevitch, H. Tittes, J. Tretter, M. Smirnow, C. Li, Actively Water-Cooled Plasma Facing Components of the Wendelstein 7-X Stellarator, Fusion Sci. Technol. 64 (2) (2013) 263–268.

[8] H.-S. Bosch, T. Andreeva, R. Brakel, T. Brauer, D. Hartmann, A. Holtz, T. Klinger, H. Laqua, M. Nagel, D. Naujoks, K. Risse, A. Spring, T.S. Pedersen, T. Rummel, P. van Eeten, A. Werner, R. Wolf, Engineering Challenges in W7-X: Lessons Learned and Status for the Second Operation Phase, IEEE Trans. Plasma Sci. 46 (5) (2018) 1131–1140.

[9] G. Maddaluno, S. Almaviva, L. Caneve, F. Colao, V. Lazic, L. Laguardia, P. Gasior, M. Kubkowska, Detection by LIBS of the deuterium retained in the FTU toroidal limiter, Nucl. Mater. Energy 18 (2019) 208–211.

[10] M. Hubeny, D. Hoschen, O. Neubauer, R. Hoek, G. Czymek, D. Naujoks, D. Hathiramani, D. Bardawil, B. Unterberg, R. Konig, S. Brezinsek, C. Linsmeier, X. Team, Progress on MATEO probe heads and observation system, Fusion Eng. Des. (2021) 5.

[11] G.S. Maurya, A. Marín-Roldán, P. Veis, A.K. Pathak, P. Sen, A review of the LIBS analysis for the plasma-facing components diagnostics, J. Nucl. Mater. 541 (2020) 152417.

[12] M. Dong, X. Mao, J.J. Gonzalez, J. Lu, R.E. Russo, Carbon Isotope Separation and Molecular Formation in Laser-Induced Plasmas by Laser Ablation Molecular Isotopic Spectrometry, Anal. Chem. 85 (5) (2013) 2899–2906.

[13] A.A. Bol'shakov, X. Mao, J.J. González, R.E. Russo, Laser ablation molecular isotopic spectrometry (LAMIS): current state of the art, J. Anal. At. Spectrom. 31 (1) (2016) 119–134.

[14] A.P. Thorne, Spectrophysics, Springer Netherlands, Dordrecht, 1988.

[15] S. Brezinsek, A. Pospieszczyk, G. Sergienko, P. Mertens, U. Samm, Use of a High-Resolution Overview Spectrometer for the Visible Range in the TEXTOR Boundary Plasma, Plasma Fusion Res. 3 (2008) S1041.

[16] C.M. Western, PGOPHER: A program for simulating rotational, vibrational and electronic spectra, J. Quant. Spectrosc. Radiat. Transfer 186 (2017) 221–242.

[17] J. Tennyson, S.N. Yurchenko, A.F. Al-Refaie, E.J. Barton, K.L. Chubb, P.A. Coles, S. Diamantopoulou, M.N. Gorman, C. Hill, A.Z. Lam, L. Lodi, L.K. McKemmish, Y. Na, A. Owens, O.L. Polyansky, C. Sousa-Silva, D.S. Underwood, A. Yachmenev, E. Zak, The ExoMol database: molecular line lists for exoplanet and other hot atmospheres, J. Mol. Spectrosc. 327 (2016) 73–94, arXiv:1603.05890.

[18] R.K. Janev, D. Reiter, Collision Processes of Hydrocarbon Species in Hydrogen Plasmas. Part 2. The Ethane and Propane Families, ChemInform 34 (37) (2003) _eprint: https://onlinelibrary.wiley.com/doi/pdf/10.1002/chin.200337260.

[19] A. Mutzke, W. Eckstein, R. Dohmen, K. Schmid, U.v. Toussaint, R. Schneider, G. Bandelow, SDTrimSP Version 600, Technical report IPP–2019-02, Germany, 2019, p. 92.